



An investigation on the falling film thickness of sheet flow over a completely wetted horizontal round tube surface

Qinggang Qiu^a, Xiaojing Zhu^a, Lin Mu^{a,b}, Shengqiang Shen^{a,*}

^aSchool of Energy and Power Engineering, Dalian University of Technology, Dalian 116024, China, Tel. +86 13591105818; email: qggang@dlut.edu.cn (Q. Qiu), Tel. +86 18642809658; email: xiaojingxjtu@126.com (X. Zhu), Tel. +86 13889636419; email: lm@dlut.edu.cn (L. Mu), Tel. +86 411 84708464; email: zzbshen@dlut.edu.cn (S. Shen)

^bKey Laboratory of Industrial Ecology and Environmental Engineering of Ministry of Education, School of Environmental Science and Technology, Dalian University of Technology, Dalian 116024, China

Received 6 January 2015; Accepted 29 July 2015

ABSTRACT

An investigation was performed to analyze the liquid film distributions of sheet flow on the surface of a horizontal round tube in a falling film evaporator using the commercial computational fluid dynamic code Fluent 6.3.26. A two-dimensional multi-phase flow model was developed under adiabatic condition. The temporal variation of flowing process of sheet flow and the steady film thickness distribution in the circumferential direction were analyzed in detail. The main objective has focused on the effects of multiple factors on the film thickness distribution. It was found that the whole process of liquid film flowing along the horizontal tube surface includes the transient sub-process and steady-state sub-process, and the former can be divided into five stages to be analyzed. The obviously asymmetric distribution of film thickness, which is contradictory to the Nusselt theory, is captured by the simulation results. Multiple factors have effects on the film thickness distribution. The film thickness increases with the increase in film Reynolds number. The big inter-tube spacing is capable of inducing high momentum and increasing the impact velocity of liquid film on the top of the tube, which results in the thinner distribution of liquid film layer around the perimeter of the horizontal tube. The film thickness becomes thinner as tube diameter increases. The effect of tube diameter is minor and the further increment of tube diameter shows few values to the improvement of heat and mass transfer.

Keywords: Horizontal round tube; Falling film; Film thickness characteristic; Sheet flow; Parameter effect

1. Introduction

Falling liquid film on the surface of a horizontal tube is an important widely existent heat and mass transfer process in modern heat exchangers. It is advantageous because of high heat transfer rate, low

film flow rates, small temperature difference, high heat transfer coefficients, and simple structure. It also offers advantages in dealing with liquid distribution, non-condensable gases, fouling, and many other operating problems of the heat exchangers [1–4]. As a kind of energy-saving distillation technology, the technology of falling film horizontal-tube evaporation has been utilized widely in desalinating seawater in recent

*Corresponding author.

years. Due to the small heat consumption of the process, the heat resource requirements are low enough to utilize low-grade waste heat [5], which is significant in alleviating the increasing energy crisis that the people all over the world have to face every day.

In a falling film horizontal-tube evaporator, the liquid to be evaporated is sprayed downward onto the top of a horizontal tube bundle, flows around the tubes in the form of thin film, and then falls freely from tube to tube. This process is accompanied by the heat transfer through the liquid–air interface since the thin, liquid film is usually exposed to the air space, as shown in Fig. 1. In order to augment the heat and mass transfer of falling film flowing over the horizontal tube, the liquid film flow should fully wet the heat transfer surface of horizontal tube. Otherwise, the so-called “dry spot” or “dry zone” might appear due to the liquid film rupture on the heat transfer surface, which very likely leads to a variety of serious consequences, such as the fouling and corrosion problems during desalination process.

The film thickness is of key importance to characterize the falling film and heat transfer phenomena over horizontal tubes. Since the heat transfer through film mainly depends on the convection and conduction [6], the circumferential thickness of a liquid film is inversely proportional to the local heat transfer coefficient. Therefore, it requires a deeper insight into the film thickness distribution to promote the development of this technology. Up to now, a number of studies in this very field have been carried out by many researchers. Nusselt [7] conducted an analytical study with a continuous sheet flow from tube to tube, and proposed following classic expression to calculate the

film thickness with neglecting the momentum effects on the falling films:

$$\delta = \left(\frac{3\mu_L \Gamma}{\rho_L(\rho_L - \rho_G)g \sin \beta} \right)^{1/3} \quad (1)$$

where Γ is the liquid film flow rate on one side per unit length of round tube and β is the circumferential angle measured from the top of a horizontal tube. The film Reynolds is defined as follow:

$$\text{Re} = \frac{4\Gamma}{\mu_L} \quad (2)$$

Rogers et al. [8,9] proposed another correlation of falling film thickness using integration method:

$$\delta = \left(\frac{3\mu_L \Gamma}{\rho_L^2 g \sin \beta} \right)^{1/3} \quad (3)$$

It can be clearly seen from above correlations that the film thickness of upper half of horizontal tube is quite symmetric to that of lower half. Mitrovic [10] investigated the flow mode transitions of adiabatic and non-phase change falling film over plain tubes and indicated the transition boundaries in the form of Reynolds number. Additional experimental observations were made by Hu and Jacobi [11] for the flow characteristics and mode transitions of the falling film on horizontal tube. The effects of several factors were captured in the film Reynolds number and a modified Galileo number and more refined flow classifications were presented. Zhang et al. [12] proposed an optical-electronic method for measurement of falling film thickness. The method was proved to be convenience, non-invasive, higher spatial, and temporal resolution in comparison with popular conductance parallel-wire probes and the maximum relative deviation between the experimental and calculated results is about 18%. Xu et al. [13,14] studied the flowing state of liquid films over horizontal tubes and analyzed the factors influencing the film thickness. The correlations to predict the heat transfer film coefficients outside the horizontal tubes, with the consideration of film-thickness influence and its fluctuation on the heat transfer, were set up by the regression of experimental data. Nosoko et al. [15] experimentally studied the characteristics of falling film flow on completely wetted horizontal tubes of 16 mm diameter in a vertical row in the Reynolds number range of 10–150. The continuous sheets between the tubes were found when the inter-tube spacing is 2 mm and clear appearance of random

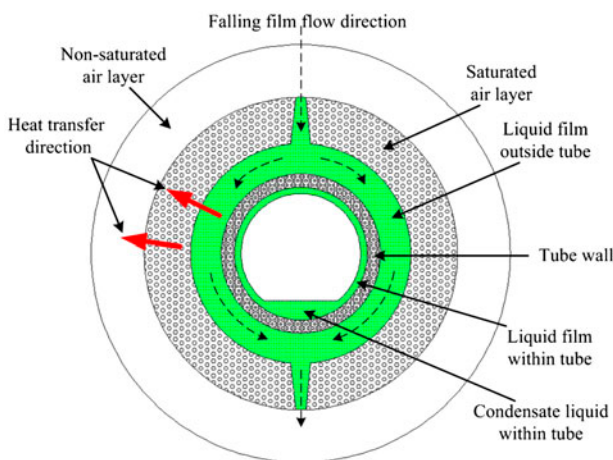


Fig. 1. Illustration of heat transfer processes associated with liquid film falling on a horizontal tube.

wave on the liquid film surface was observed when $Re > 30$. Gstoehl et al. [16] obtained the variation rules of film thickness of sheet flow within circumferential angles from 0° to 160° using non-contact laser measurement technique. Their experimental results showed that the prediction of film thickness by Nusselt [7] is pretty well with the upper part of tube circle. While for the lower part of tube circle, the prediction is overestimated compared with the experimental results. It means that the conclusion of symmetric distribution in the circumferential direction of horizontal tube is not accurate based on the experimental results obtained by Gstoehl et al. [16]. This point of view is also supported by Wang et al. [17] who conducted the non-intrusive measurement of falling film thickness on the perimeter of both horizontal Turbo-CII tube and plain tube. Hou et al. [18] performed an experimental investigation of liquid film falling around a horizontal tube and used a displacement micrometer to determine the distribution characteristics of the film thickness. The effects of circumferential angle, inter-tube spacing, and film Reynolds number on the distribution characteristics were discussed in detail. It was found that the minimal values of the film thickness locate at different circumferential angles in the range of $90\text{--}115^\circ$ rather than at the single point of 90° predicted by Nusselt. The following modified correlation on the basis of Nusselt correlation was derived to correlate the experimental data:

$$\delta = C \left(\frac{3\mu_L \Gamma}{\rho_L(\rho_L - \rho_G)g \sin \beta} \right)^{1/3} \left(\frac{s}{D} \right)^n \quad (4)$$

where s is the inter-tube spacing, D is the outside diameter of tube, and C is the correction factor of which the value is determined by the circumferential angles.

In addition to the experimental research, the researches based on computational fluid dynamic (CFD) were also introduced to this field. Min and Choi [19] developed a Navier–Stokes procedure to study the absorption phenomena about the free-falling film flow on a horizontal tube. The variations of stagnation film thickness, as well as the circumferential film thickness distribution, vs. Re number and surface tension were revealed. It was found that the calculated film thickness agrees well with the Nusselt [7] solution when the flow rate is low. However, the differences between them become larger as the flow rate increases and the reason was attributed to the longer time spend to attain the fully developed state. Apparently, simulation results by Min

and Choi did not capture the circumferential differences of film thickness around the horizontal tube. Killion and Garimella [20] conducted a computational model to predict the behavior of falling films and droplets in horizontal tube banks. The details of falling film, droplet formation, as well as the fall and impact process were revealed by the model. It was reported that the calculated surface area and volume of the droplet well agreed with the results from their visualization studies [21,22]. Subramaniam and Garimella [23] performed a numerical study of heat and mass transfer in lithium bromide water falling films and droplets. It was found that the flow over tube banks actually occurs as wavy films on the tube surface and as droplets in the inter-tube space. The formation and detachment of these droplets, and their impact on the tube affect heat and mass transfer considerably.

Based on above researches, it can be seen that the distribution characteristics of falling film thickness, along with the heat and mass transfer characteristics over horizontal tube bundles have been serially and systematically studied. The experimental method is usually the first choice for many researchers to explore this field since the experiment-based data with certain accuracy is more objective, visualized, and reliable to be used in engineering design. As mentioned above, the distribution characteristic of falling film thickness is closely related to the local heat transfer coefficient which is a crucial factor for the desalination efficiency of horizontal-tube evaporator. It is synthetically affected by thermodynamic parameters and structural parameters of the system. Therefore, the effects of these parameters on the falling film thickness distribution need to be further cleared. However, it costs pretty much in both time and money to acquire fully and deeply knowledge through experimental method. The numerical method, on the other hand, has distinct advantages of revealing the fine, detailed information, as well as the comprehensive influence mechanism of falling film evaporation process with much less cost in comparison with experimental research.

In this paper, the commercial CFD code Fluent 6.3.26. is used as working platform to investigate the falling film distribution of sheet flow over horizontal tubes. Based on our earlier research [24], the contents in this paper further focus on the analysis of the main influence factors, including the thermodynamic parameters and structural parameters, and revealing the corresponding mechanism involved in the flowing process. The results may provide a basis and guidance for further research and development of efficient horizontal-tube falling film evaporator.

2. Numerical approach

2.1. Analysis geometry and physical conditions

It is assumed here that the falling film flow on the horizontal tube surface is an incompressible, low-velocity, and viscous sheet flow driven by gravity. The assumption allows the standard form of the Navier–Stokes equations to be adopted in this paper. The properties of the surrounding gas phase, air, and the liquid phase, water, are assumed to be constant under the normal condition with temperature of 25°C and pressure of 101.325 kPa. The summarized properties of air and water are listed in Table 1.

As shown in Fig. 2, the tube bundle studied here is horizontally arranged, and the shaded region is chosen as the solution domain to save the computing time considering the symmetrical geometry. The solution domain is discretized by quadrilateral elements, as shown in Fig. 3. A boundary layer technique for the region near the tube wall, as well as the very fine meshes for the region where the two-phase flow is involved, is used to precisely capture the detailed

Table 1
Summary of fluid properties used in computational analysis

	ρ (kg m ⁻³)	μ (kg m ⁻¹ s ⁻¹)	σ (N m ⁻¹)
Water	998.2	1×10^{-3}	0.073
Air	1.225	1.7894×10^{-4}	–

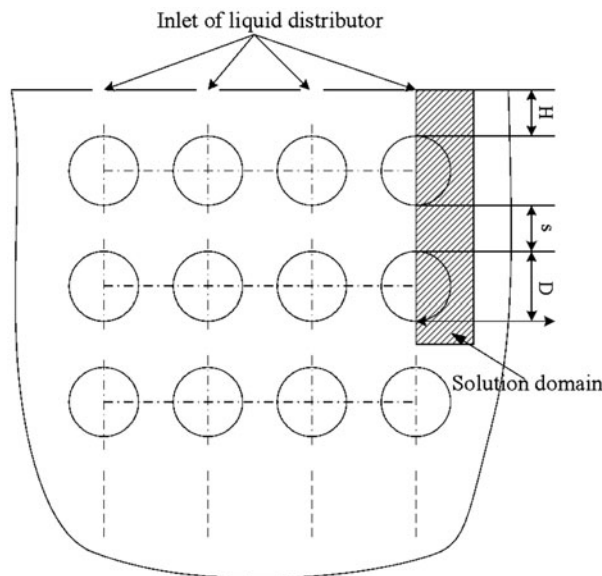


Fig. 2. Sketch of structure for falling film horizontal-tube evaporator.

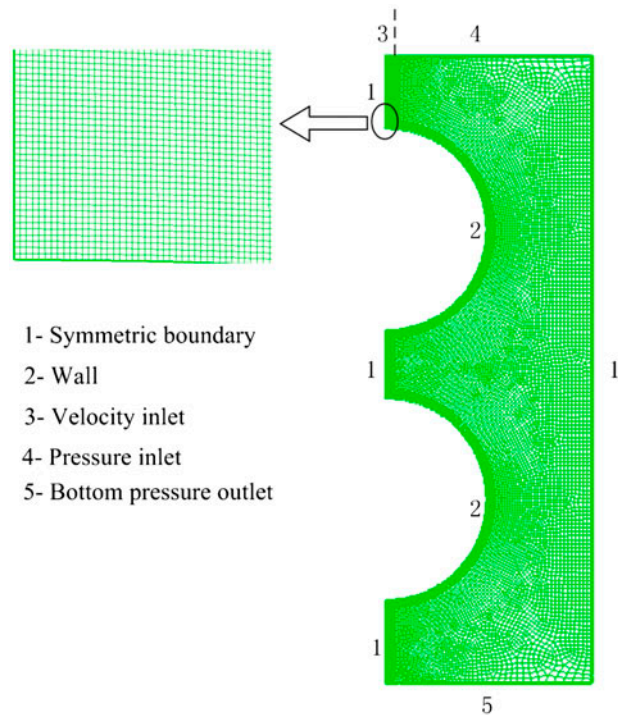


Fig. 3. The boundary conditions and 2D grid of the solution domain.

information of the mass transfer process around the horizontal tube. On the top of the solution domain, the left-most part (refer to Fig. 3), which represents the liquid flow path to the top of tube, is set as the velocity inlet. And the rest of the top of the solution domain is set as the pressure inlet. The bottom of solution domain is set as pressure outlet with specified constant pressure. The tube wall is supposed to be a smooth, no-slip wall without heat flux. As the initial condition, the calculated region is set to be fully filled with air, and the volume fraction of liquid water at the entrance (velocity inlet) is set as 1.0. In addition, a wall contact angle, which is used to adjust the surface normal in the cells near the wall, is specified as 0° to ensure the complete wetting of the wall in the simulation.

2.2. Computational method

The mass conservation, as known as continuity equation, can be derived by applying Reynolds' transport theorem to any material volume. Notice that the mass within a material volume is constant for incompressible fluid and thus the derivative of the mass with respect to time equals to zero:

$$\text{div}(\mathbf{U}) = 0 \quad (5)$$

The momentum conservation is given as

$$\frac{\partial(u)}{\partial t} + \text{div}(uU) = \text{div}(v \text{grad } u) - \frac{1}{\rho} \frac{\partial p}{\partial x} + S_u \quad (6)$$

and

$$\frac{\partial(v)}{\partial t} + \text{div}(vU) = \text{div}(v \text{grad } v) - \frac{1}{\rho} \frac{\partial p}{\partial y} + S_v \quad (7)$$

where S_u and S_v , the general source terms, equal to zero for the incompressible fluid with constant viscosity.

The finite volume method is employed here to translate these coupled, partial differential equations into algebraic expressions that can be solved using a computer. In this process, the motion and continuity equations are integrated for each computational cell and then discretized with the second-order upwind scheme. The discretized equations are linearized and solved in a segregated, first-order implicit manner [20]. The pressure-implicit with splitting of operators (PISO) method is used to relate the solution of the continuity equation to the pressure correction. The volume of fluid (VOF) method presented by Hirt and Nichols [25] is used as multi-phase flow model to capture the free surface of gas–liquid two-phase flow. In present study, the gas phase, air, is defined as the principal phase of which the volume fraction is represented by α_1 , while the liquid phase, water, is defined as the second phase of which the volume fraction is represented by α_2 . The continuity equation can be slightly modified to be solved for the second phase, water:

$$\frac{\partial \alpha_2}{\partial t} + \vec{u} \cdot \nabla \alpha_2 = 0 \quad (8)$$

and the solution for the volume fraction for principal phase, air, is given as

$$\alpha_1 = 1 - \alpha_2 \quad (9)$$

where \vec{u} is the velocity vector. Based on Eqs. (8) and (9), it can be seen that a mesh cell is entirely filled with liquid for $\alpha_2 = 1$, with gas for $\alpha_2 = 0$ and with gas–liquid two phase for $0 < \alpha_2 < 1$. The properties of two phase flow in each cell can thus be obtained in the form of weighted average values:

$$\rho = \alpha_2 \rho_2 + (1 - \alpha_2) \rho_1 \quad (10)$$

$$\mu = \alpha_2 \mu_2 + (1 - \alpha_2) \mu_1 \quad (11)$$

where ρ and μ are the evaluated density and viscosity within the cell; ρ_1, ρ_2 and μ_1, μ_2 are the densities and viscosities of phase 1 and phase 2, respectively.

2.3. Mesh and time-step independence

Several cases with different mesh numbers, which widely cover from 10,000 to 111,000, are tested in this paper to fully evaluate the mesh sensitivity. The corresponding working condition is of $Re = 680$, $D = 19.05 \text{ mm}$, and $s = 6.4 \text{ mm}$. Fig. 4 shows the variations of average film thickness calculated based on different mesh numbers at the circumferential angle of 110° (refer to the sub-figure of Fig. 4). It can be seen that the calculated film thickness evidently decreases with the increase in mesh number when the mesh number is less than 70,147. It is almost constant when the mesh number is greater than 70,147, and the relative error of calculated film thickness is about 0.2% when mesh number rises from 70,147 to 111,000. It thus can be concluded that the calculations are mesh independent when the mesh number is over 70,147. Under this circumstance, the distance between two adjacent nodes of the very fine mesh near the tube wall and the region where the interface of two-phase flow is involved, represented by l in Fig. 3, equals to or less than 0.01 mm. Therefore, the corresponding mesh system is adopted as a baseline for the rest of CFD analysis based on the consideration of computational time and cost.

Since the transient process, such as the liquid flowing from the top to the bottom of a horizontal tube, is

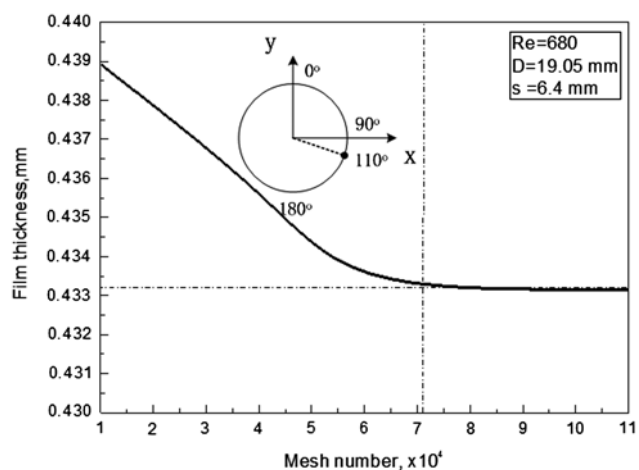


Fig. 4. Variation of film thickness calculated based on different mesh numbers.

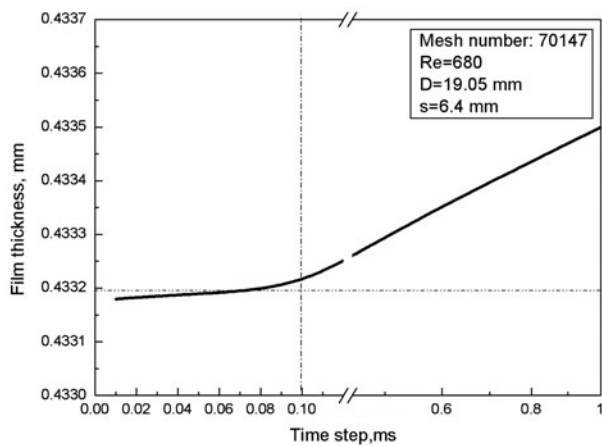


Fig. 5. Variation of film thickness calculated based on different time steps.

involved in present study, the time-step dependency study is also conducted to avoid the influences of time step on the simulation results. Fig. 5 shows the variations of film thickness calculated based on different time steps at circumferential angle of 110° . The mesh number used here is 70,147 and the corresponding working condition is of $Re = 680$ and $s = 6.4$ mm. It can be seen that the film thickness changes very little when time step is less than 0.1 ms, and the relative error of calculated result is about 0.01% in the variation range of time step from 0.01 to 0.1 ms. It can be concluded that the calculations are time-step independent when the time step is less than 0.1 ms.

2.4. Verification of computational method

It should be noticed that the physical model built in this paper is 2D in the radius direction; the extension of liquid film in the axial direction is ignored. Fig. 6 shows the calculated film thickness of sheet flow based on the Nusselt correlation [7], the measured results by Gstoehl et al. [16], and the simulated results of this paper plotted against the circumferential angles at $Re = 574$, $s = 6.4$ mm, and $D = 19.05$ mm. It can be seen that the relative error between the simulation results of this paper and the calculated results from Nusselt correlation is within 20%. And the variation trend of the simulation results of this paper agrees with the experimental data by Gstoehl well. The film thickness decreases with the increase in circumferential angle and then increases after it reaches the minimum value. The obvious, asymmetric distribution phenomenon of film thickness, which is characterized by the bigger value on the upper half and smaller value on the lower half, is also captured by the

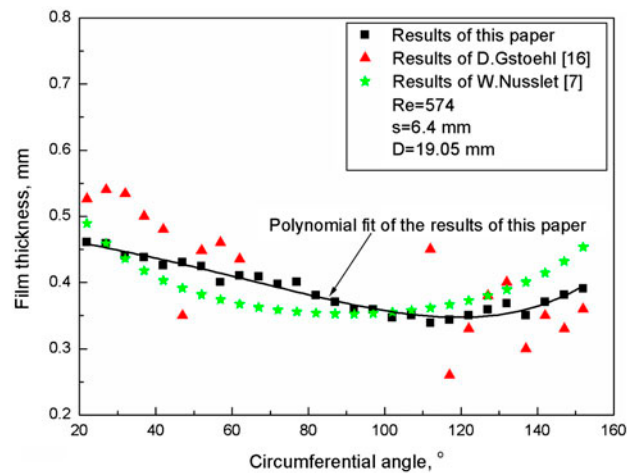


Fig. 6. Comparisons of results of this paper and the results by other researchers.

simulation result. For the upper part of the tube surface, the angular range from approximately 20° to 60° , the measured film thickness by Gstoehl is bigger than the calculated film thickness based on Nusselt correlation, while for the lower part, the angular range from approximately 110° to 160° , the results by Gstoehl is much lower than the results based on Nusselt correlation. The possible cause was attributed to the assumption of negligible momentum effects on the flow in Nusselt theory.

Despite the quantity differences between the simulation results of this paper and the results by above researchers through theoretical and experimental methods, it is proved that the 2D model along with VOF method is capable of capturing the falling film distribution of sheet flow over horizontal tube under adiabatic condition. Therefore, this method is recommended in predicting the film thickness characteristics of sheet flow over horizontal tube and adopted in the present study for following researches.

3. Numerical results and discussion

3.1. The transient process

As mentioned above, the process of liquid film flowing from the top to the bottom of a horizontal tube is a transient process, as shown in Fig. 7 at $Re = 580$, $s = 19$ mm, and $D = 19.05$ mm. The flow pattern, as well as the film thickness on the tube surface, varies over time and can be divided into five stages. The first one is the free falling stage, as shown in Fig. 7(a), $t = 0.02$ s. The liquid with a certain velocity is driven by the gravity and flows downwardly to the top of tube. The second one is the liquid impact stage,

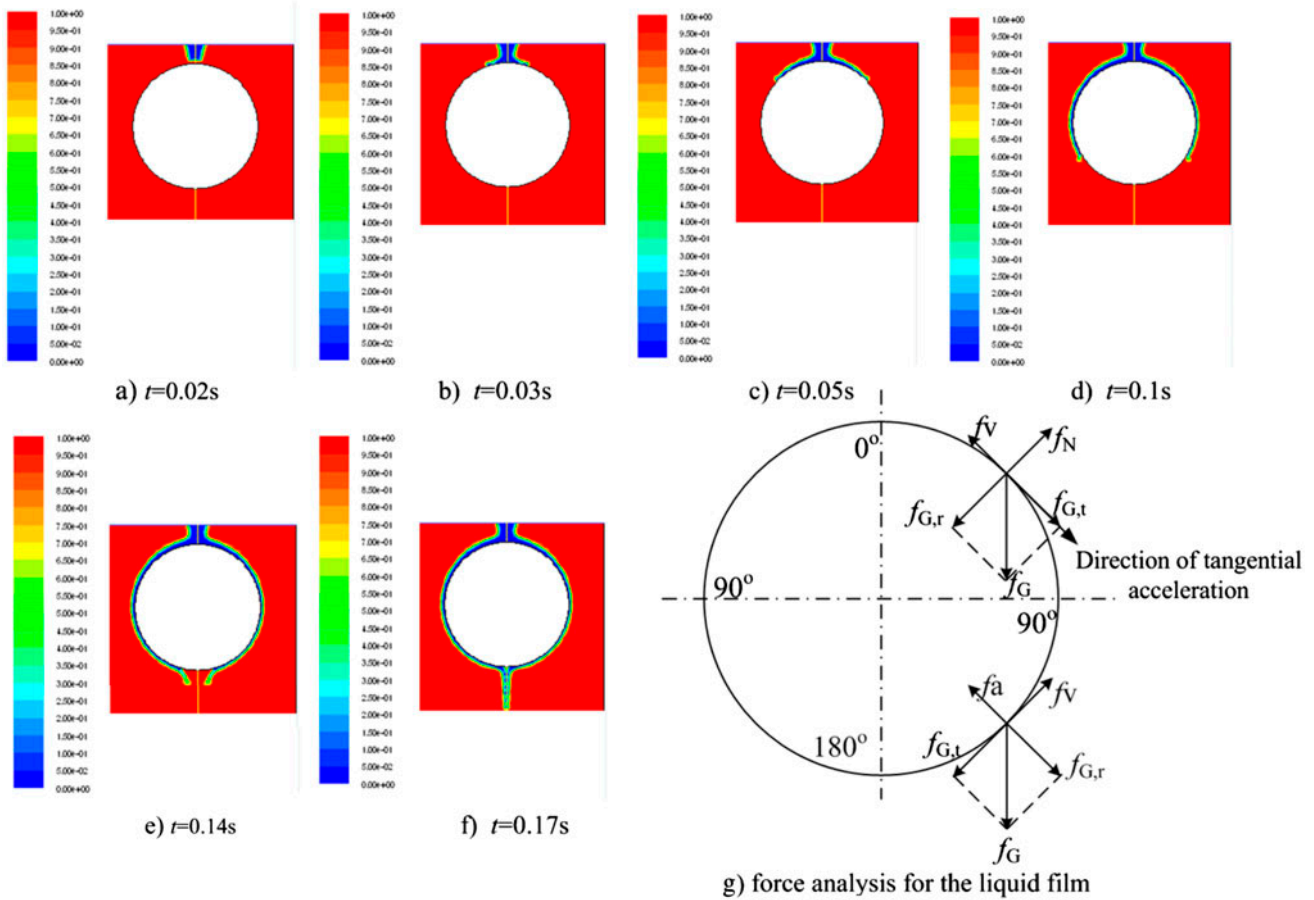


Fig. 7. Falling liquid film profile over the cylinder at different times.

as shown in Fig. 7(b), $t = 0.03$ s. The liquid reaches the top surface of the tube and gradually spreads to form the liquid film along tube surface. In this stage, the flow resistance, including the pressure loss caused by the impact process and the viscous drag between the liquid and tube surface, must be overcome to assure the formation of liquid film. Otherwise, the so-called “fracture” of liquid film may appear. The following one is the liquid film developing stage, as shown in Fig. 7(c), $t = 0.05$ s. Driven by the tangential component force of gravity, the liquid film continues to spread along the circumferential direction by overcoming the viscous drag. The fourth one is the liquid film fully developed stage, as shown in Fig. 7(d), $t = 0.1$ s. The most part of tube surface has been covered by liquid film in this stage. Because the tangential component force of gravity reaches the maximum value at the circumferential angle of 90° , the liquid film continues to accelerate and reaches its max value in the circumferential range between 90° and 140° . Accordingly, the minimum liquid film

thickness also appears in this circumferential range. The velocity of liquid film has obviously affected the film thickness distribution and this phenomenon explains the differences between the simulation results of this paper and the calculation results based on Nusselt theory which totally ignored the momentum effects on the flow. In the final stage, as shown in Fig. 7(e) and (f), $t > 0.14$ s, the tube surface has been fully covered by the liquid film. Under the synthetic action of gravity, viscous drag, surface tension, and adhesive force, the liquid departs from the bottom of tube, forms a series of liquid drop or liquid column, and flows downwardly to the top of next tube.

Based on the above results, it can be seen that the film thickness distribution on a horizontal tube surface is highly related to the circumferential position which directly determines the direction and value of tangential acceleration, as shown in Fig. 7(g). For the upper part of the tube, the tangential component force of gravity, $f_{G,t}$, equals to zero at the circumferential angle of 0° and reaches the max value, f_G , at the

circumferential angle of 90° . The radial component force of gravity, $f_{G,r}$, is balanced by the normal force from tube surface, f_N . The tangential acceleration thus varies in the same way as the tangential component force of gravity. For the lower part of the tube, the tangential component force of gravity, $f_{G,t}$, decreases from the max value, f_G , to zero along with the variation of circumferential angle from 90° to 180° . The radial component force of gravity, $f_{G,r}$, is balanced by the adhesive force, f_a . When $f_{G,t}$ decreases to the value less than the viscous drag, f_v , the tangential acceleration changes to the exactly opposite direction and this is the point that the velocity of liquid film reaches the maximum value and begins to decrease. Therefore, the circumferential velocity of liquid along the surface of horizontal tube increases from 0° to 90° , reaches the maximum value in the range between 90° and 140° , and then decreases till the very bottom, 180° , is reached or the liquid departs from the tube surface. The variation rule of velocity is quite corresponding to the film thickness distribution showed in Fig. 6, indicating a certain relevance between the film thickness distribution and circumferential velocity.

3.2. Analysis of parameter effect

When the tube surface is fully covered by the liquid film, the distribution of liquid film on the tube surface can be considered as a steady state with constant boundary conditions. According to the Nusselt theory, the film thickness distribution is the function of circumferential position and affected by several factors, such as the physical property of liquid and film Reynolds number. In addition, the inter-tube spacing, s , and the tube diameter, D , also have effects on the film thickness distribution for tube bundle condition.

Fig. 8 shows the effect of Reynolds number on the film thickness distribution in the circumferential direction of a horizontal tube. Three cases with different Reynolds numbers, 480, 680, and 880, are tested. It is clearly seen that the circumferential distributions of film thickness for all three cases are similar to each other. With the increment of circumferential angle, the film thickness decreases first, and then increases after the minimum value, which appears in the circumferential range between 100° and 140° , is reached. However, the Reynolds number does affect the amount of the film thickness. For instance, the film thickness rises from approximately 0.45 to 0.6 mm at circumferential angle of 20° when Reynolds number rises from 480 to 880. This simulation result is consistent with the experimental result by Hou et al. [18], who has verified the effect laws of Reynolds number on film thickness using displacement micrometer.

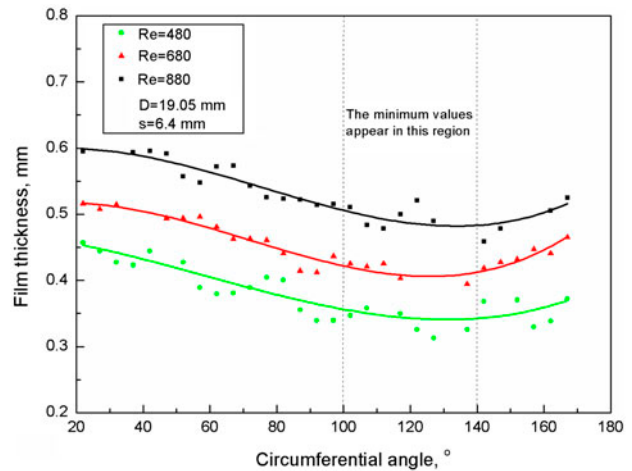


Fig. 8. Film thickness distribution vs. circumferential angle at different Reynolds numbers.

The velocity (m/s) refers to the speed of liquid film relative to the stationary tube surface. At the time when the liquid is just about to impact the top of the tube, the velocity depends not only on the film Reynolds number (or mass flow rate), but also on the inter-spacing between this tube and the one above it. The bigger the spacing is, the higher the velocity is. Fig. 9 shows the film thickness at the given circumferential position, 45° , of the lower tube surface vs. Reynolds number at different inter-tube spacings, 6, 9, 12, and 19 mm, between the lower tube and the one above it. The Reynolds number refers to the initial Reynolds number assigned to the upper tube. It can be seen that the film thickness increases with the increasing film Reynolds number for each inter-tube

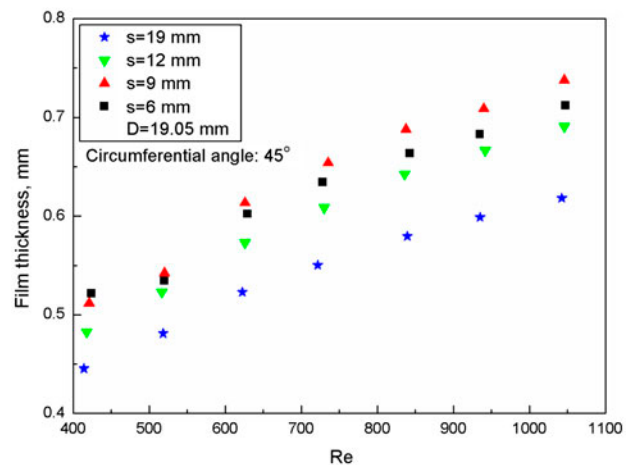


Fig. 9. Film thickness vs. Reynolds number at different inter-tube spacings.

spacing studied. In general, the film thickness decreases with an increase in tube spacing at a given Reynolds number. When the tube spacing is further increased to 19 mm, the film thickness decreases by approximately 15% in comparison with that when the tube spacing is 6 mm. This phenomenon is logically because of the added momentum of the falling liquid [16]. Based on the data in Fig. 9, it can be concluded that big inter-tube spacing is capable of inducing high momentum and increasing the impact velocity of liquid film on the very top of the tube. The liquid mass per unit area at a given film Reynolds number is thus reduced, which results in the thinner liquid film layer around the perimeter of the horizontal tube.

The diameter of tube is an important structure parameter that relates to the heat transfer efficiency and manufacture cost of a falling film horizontal-tube evaporator. However, it is not easy to fully evaluate the effect of tube diameter through experimental method because widely changing the diameter of test tube can cause very high cost in both time and money. Therefore, very few experimental researches have been reported to reveal the relevant features. In present study, the effect of tube diameter on the falling film thickness is discussed and the wide tube diameter

range, 19–90 mm, has been covered. The corresponding simulation results are diagrammatically illustrated in Fig. 10(a) and quantitatively shown in Fig. 10(b).

It can be seen from Fig. 10(a) that the film thickness, represented by blue color, obviously changes with different tube diameters. The local film thickness at certain circumferential position decreases when the tube diameter is increased. The curvature of circumference is small for the tube with big diameter. Since the liquid film flows along the tangential direction of tube surface, both the direction and amount of its velocity change slower because of the smaller curvature. Fig. 10(b) shows the film thickness vs. tube diameter at different Reynolds numbers. The film thickness decreases with an increase in tube diameter. This phenomenon may be explained as follows: the bigger diameter means longer arc length for the liquid film to flow in a certain circumferential angle range. The velocity of liquid film is thus higher at the certain circumferential position for the tube with bigger diameter. As mentioned in Section 3.1 of this paper, the film thickness distribution is relevant to the film velocity along tube surface. The higher the velocity is, the thinner the liquid film is. In addition, it also can be seen from Fig. 10(b) that the changing ways of film

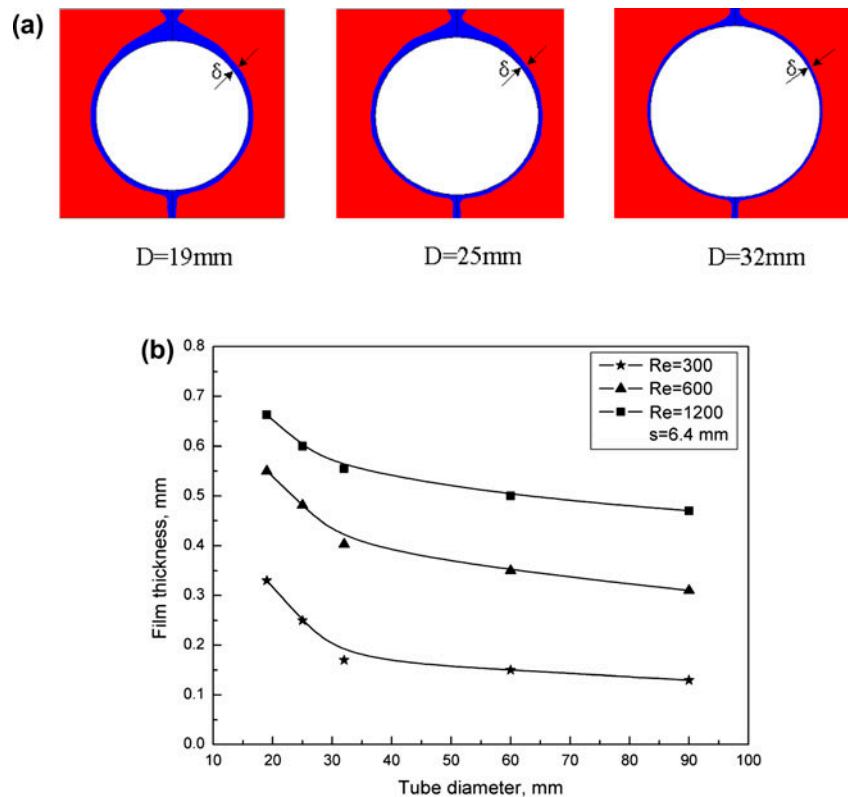


Fig. 10. Film distribution around the horizontal tube for (a) illustration of liquid film distribution with different diameters and (b) film thickness vs. tube diameter at different Reynolds numbers.

thickness in different diameter ranges are distinguishable. Take the case of $Re = 600$ as an example. The film thickness decreases from 0.55 to 0.4 mm when the tube diameter increases from 19 to 32 mm. The change rate of film thickness with respect to the tube diameter can be defined as follows:

$$\varepsilon = \Delta\delta/\Delta D \quad (12)$$

where $\Delta\delta$ is the film thickness differential and ΔD is the tube diameter differential, respectively. The corresponding change rate is approximately 0.115 in the range between 19 and 32 mm, while it is approximately 0.00172 in the range between 32 and 90 mm. It means that the tube diameter greatly affects the film thickness distribution within a certain tube diameter range, in this case, less than 32 mm. When the tube diameter is greater than 32 mm, the effect of tube diameter is minor and hence, the further increment of tube diameter shows few values to the improvement of heat and mass transfer.

For the case with film Reynolds number of 300, as also can be seen in Fig. 10(b), the film thickness is close to 0.1 mm when the tube diameter is greater than 32 mm. This is definitely a very small value and even a small fluctuation of liquid film, which very likely appears in a falling film evaporator, can cause the fracture of liquid film on the tube surface. Therefore, the liquid flow rate must match with the tube diameter to meet the engineering requirement of falling film evaporator.

4. Concluding remarks

Using commercial CFD code Fluent as working platform, this paper conducts a numerical investigation on the film thickness distribution characteristics over horizontal tubes within a falling film evaporator under adiabatic condition. The main objective has focused on the transient process of liquid film falling from the top to the bottom of tube and the effects of multiple factors on the film thickness distribution. Some main conclusions achieved so far are summarized below:

- (1) The process of liquid flowing on the horizontal tube surface includes two main sub-processes which are transient and steady, respectively. The transient sub-process starts with the stage of free falling from the liquid distributor inlets or the bottom of upper tube, and then experiences the liquid impact stage, liquid film developing stage, liquid film fully developed

stage and finally ends up with the stage that liquid film fully covers the tube surface and flows downwardly to the top of next tube.

- (2) The liquid film distribution is in steady after the tube surface is fully covered under the constant boundary conditions. The circumferential distribution of film thickness along tube surface is not uniform. It decreases from the very top of the horizontal tube and then increases after it reaches the minimum value which approximately appears within the circumferential angle range between 100° and 140° . The asymmetric distribution, which is contradictory to the Nusselt theory, is supported by the results of several experimental researches.
- (3) The circumferential distribution trend of film thickness on the tube surface corresponds to the variation trend of liquid film velocity, indicating that the momentum effect on the flow cannot be ignored. The big inter-tube spacing is capable of inducing high momentum and increasing the impact velocity of liquid film on the top of the tube. The liquid mass per unit area at a given film Reynolds number is thus reduced, which results in the thinner liquid film layer around the perimeter of the horizontal tube.
- (4) The film thickness decreases with the increase in tube diameter, and the changing ways in different diameter ranges are distinguishable. When the tube diameter is greater a certain value, effect of tube diameter is minor and the further increment of tube diameter thus shows few values to the improvement of heat and mass transfer.

Acknowledgements

The authors acknowledge the financial support of the National Natural Science Fund of China (51336001). The authors thank the anonymous reviewers for their helpful comments and suggestions related to this paper.

Nomenclature

C	—	correction factor
D	—	diameter (mm)
G	—	acceleration of gravity (m/s^2)
H	—	vertical distance between the liquid distributor and the top of the first row of tube (mm)
P	—	pressure (Pa)
Re	—	Reynolds number
S	—	inter-tube spacing (mm)
S	—	source item
T	—	time (s)

U	— velocity scale in x direction
\mathbf{U}	— velocity vector
V	— velocity scale in y direction
X	— length scale
Y	— length scale
α	— volume fraction
β	— circumferential angle ($^\circ$)
δ	— liquid film thickness (m)
σ	— surface tension (N/m)
μ	— dynamic viscosity (kg/ms)
ν	— kinematic viscosity (m^2/s)
Γ	— liquid film flow rate on one side per unit length of round tube (kg/ms)
ρ	— density (kg/m^3)
<i>Subscript</i>	
1	— the primary phase
2	— the second phase
L	— liquid
G	— gas

References

- [1] Y. Fujita, M. Tsutsui, Experimental investigation of falling film evaporation on horizontal tubes, *Heat Transfer Jpn. Res.* 27 (1998) 609–618.
- [2] A.M.I. Mohamed, Flow behavior of liquid falling film on a horizontal rotating tube, *Exp. Therm. Fluid Sci.* 31 (2007) 325–332.
- [3] Z. Liu, Q.Z. Zhu, Y.M. Chen, Evaporation heat transfer of falling water film on a horizontal tube bundle, *Heat Transfer Asian Res.* 31 (2002) 42–55.
- [4] G. Ribatski, A.M. Jacobi, Falling-film evaporation on horizontal tubes—A critical review, *Int. J. Refrig.* 28 (2005) 635–653.
- [5] L. Xu, M. Ge, S.C. Wang, Y.X. Wang, Heat-transfer film coefficients of falling film horizontal tube evaporators, *Desalination* 166 (2004) 223–230.
- [6] L.P. Yang, S.Q. Shen, Experimental study of falling film evaporation heat transfer outside horizontal tubes, *Desalination* 220 (2008) 654–660.
- [7] W. Nusselt, Die Oberflächenkondensation des Wasserdampfes *Zeitschr* (The surface condensation of water vapour), *Ver. Deut. Ing.* 60(541–546) (1916) 569–575 (in Germany).
- [8] J.T. Rogers, Laminar falling film flow and heat transfer characteristics on horizontal tubes, *Can. J. Chem. Eng.* 59 (1981) 213–222.
- [9] J.T. Rogers, S.S. Goindi, Experimental laminar falling film heat transfer coefficients on a large diameter horizontal tube, *Can. J. Chem. Eng.* 67 (1989) 560–568.
- [10] J. Mitrovic, Influence of tube spacing and flow rate on heat transfer from a horizontal tube to a falling liquid film, in: *Proc. 8th International Heat Transfer Conf.*, vol. 4, San Francisco, CA, 1986, pp. 1949–1956.
- [11] X. Hu, A.M. Jacobi, The intertube falling film: Part 1—Flow characteristics, mode transitions, and hysteresis, *J. Heat Transf.* 118 (1996) 616–625.
- [12] J.T. Zhang, B.X. Wang, X.F. Peng, Falling liquid film thickness measurement by an optical-electronic method, *Rev. Sci. Instrum.* 71 (2000) 1883–1886.
- [13] L. Xua, S.C. Wang, Y.X. Wang, Y. Ling, Flowing state in liquid films over horizontal tubes, *Desalination* 156 (2003) 101–107.
- [14] L. Xu, S.Y. Wang, S.C. Wang, Y.X. Wang, Studies on heat-transfer film coefficients inside a horizontal tube in falling film evaporators, *Desalination* 166 (2004) 215–222.
- [15] T. Nosoko, A. Miyara, T. Nagata, Characteristics of falling film flow on completely wetted horizontal tubes and the associated gas absorption, *Int. J. Heat Mass Transfer* 45 (2002) 2729–2738.
- [16] D. Gstoehl, J.F. Roques, P. Crisinel, J.R. Thome, Measurement of falling film thickness around a horizontal tube using a laser measurement technique, *Heat Transfer Eng.* 25 (2004) 28–34.
- [17] X.F. Wang, M.G. He, H.L. Fan, Y. Zhang, Measurement of falling film thickness around a horizontal tube using laser-induced fluorescence technique. The 6th international symposium on measurement techniques for multiphase flows, *J. Phys.: Conf. Ser.* 147 (2009) 1–8.
- [18] H. Hou, Q.C. Bi, H. Ma, G. Wu, Distribution characteristics of falling film thickness around a horizontal tube, *Desalination* 285 (2012) 393–398.
- [19] J.K. Min, D.H. Choi, Analysis of the absorption process on a horizontal tube using Navier-Stokes equations with surface-tension effects, *Int. J. Heat Mass Transfer* 42 (1999) 4567–4578.
- [20] J.D. Killion, S. Garimella, Simulation of pendant droplets and falling films in horizontal tube absorbers, *J. Heat Transfer* 126 (2005) 1003–1013.
- [21] J.D. Killion, S. Garimella, Gravity-driven flow of liquid films and droplets in horizontal tube banks, *Int. J. Refrig.* 26 (2003) 516–526.
- [22] J.D. Killion, S. Garimella, Pendant droplet motion for absorption on horizontal tube banks, *Int. J. Heat Mass Transfer* 47 (2004) 4403–4414.
- [23] V. Subramaniam, S. Garimella, Numerical study of heat and mass transfer in lithium bromide-water falling films and droplets, *Int. J. Refrig.* 40 (2014) 211–226.
- [24] Q.G. Qiu, W.G. Jiang, S.Q. Shen, X.J. Zhu, X.S. Mu, Numerical investigation on characteristics of falling film in horizontal-tube falling film evaporator, *Desalin. Water Treat.* (2014) 1–6, doi:10.1080/19443994.2014.968907.
- [25] C.W. Hirt, B.D. Nichols, Volume of fluid (VOF) method for the dynamics of free boundaries, *J. Comput. Phys.* 39 (1981) 201–225.